Fermilab Library
0 1160 0052548 9

SDC-90-00107

# SDC
# SOLENOIDAL DETECTOR NOTES

## DESIGN OF A LIQUID ARGON CALORIMETER FOR SDC

KEK and Kawasaki Heavy Industry Co. Ltd.
Presented by Y. Unno

Proceedings of the Int'l Workshop on Solenoidal Detectors for the SSC,
KEK, Tsukuba, Japan, April 23-25, 1990

Proceedings of the International Workshop on Solenoidal Detectors for the SSC
KEK, Tsukuba, Japan, April 23-25, 1990

# Design of a Liquid Argon Calorimeter for SDC

KEK and Kawasaki Heavy Industry Co. Ltd

*Presented by Y.Unno*
*Department of Physics, KEK*
*Tsukuba, Ibaraki 305, Japan*

Abstract

The structural design of a Liquid Argon Calorimeter for the Solenoidal Detector Collaboration (SDC) has been developed through joint work between KEK and Kawasaki Heavy Industry. Cryostat wall thicknesses, concepts for cold mass support, and close-out of the cryostat are presented. A scheme of lateral and longitudinal segmentation is given and the number of readout channels are presented. Capacitances of the EM and HAD segments are evaluated along with signal speed, limitations of the cables, and thermal noise. Implications for the interleaving of HAD segments and location of preamps are discussed.

## *1. Introduction*

Liquid calorimetry using the liquid argon as an ionization medium of the calorimeter has many advantages such as; 1) durability in a high radiation environment, 2) ease of absorber/readout segmentation, 3) linear, uniform, and stable response, 4) straightforwardness in precision charge injection, 5) simple calibration which is a result of 3) and 4), 6) capability of operation in a magnetic field, and 7) well-established technology.

To establish the liquid argon calorimeter (LAC) as a viable candidate for the SDC detector, we must demonstrate that the physics performance is acceptable despite; a) the presence of dead material due to the cryostat

walls and support structures (hermeticity), and b) slow drift speed of electrons in the liquid argon (speed of response).

Recognizing that the engineering issues are critical, KEK and KHI[1] have been working on an engineering model and have proposed a candidate LAC design. Our first presentation was made to the SDC collaboration meeting at Dallas, March 11-13, 1990, and this is a progress report.

## *2. Design of the cryostat*

Although an engineering design study of a LAC for SSC has been done[2], the design is not strictly applicable for the SDC. The superconducting magnet was to be placed outside of the calorimeter. In the ACS design[3], the magnet is inside of the calorimeter. This magnet location offers added flexibility to the design of the calorimeter, but trade-offs are more complex.

*Design conditions*: Design operating conditions for the cryostat are tabulated in Table 1. The differential pressure on the wall of the inner vessel (LAr vessel), $\Delta p_{LA}$, is +3.9kg/cm$^2$ under the normal operation and -1.0kg/cm$^2$ when the inside is evacuated to purify the internal volume. The differential pressure on the wall of the outer vessel (Vacuum vessel), $\Delta p_V$, is -1.0kg/cm$^2$ under the normal operation and +0.85kg/cm$^2$ in case a liquid argon spill occurs due to breakage of the LAr vessel. We assume the same design pressures as in the Martin Marietta engineering study.

The whole calorimeter is composed of one Barrel, and two Endcap calorimeters. We assume lead as the converter, with a calorimeter thickness of approximately 8 interaction lengths (live with lead and liquid argon). The weight of the calorimeter is roughly estimated and tabulated in the table. For the calorimeter vessels, we choose to use 5083 aluminum alloy. This alloy has more than twice the strength per radiation length of Stainless Steel and excellent welding characteristics.

To obtain suitable vessel wall thicknesses and strength, we utilize; (1) the formulae in the ASME Boiler and Pressure Vessel Code Sec. VIII. Div.2; (2) a finite element method (FEM) of analysis for axially symmetric shells developed by KHI; and (3) 3-dimensional FEM analysis. We are in stage (2)

and 3-dimensional analysis has just begun. The vessel's primary stresses are required to be less than the maximum allowable stress ($S_m$~7kg/mm$^2$) and the secondary stresses less than $3S_m$. Instability is being evaluated with FEM. Structural analysis is still in progress and the numbers given in this report are preliminary although they are converging.

Table 1. Design conditions for the LAr Calorimeter

| | |
|---|---|
| Differential pressures: | |
| LAr vessel ($\Delta p_{LA}$) | +3.9[(a)] / -1.0[(b)] kg/cm$^2$ |
| Operating pressure | +0.7 / -1.0 |
| Safety relief pressure | +0.4 |
| LAr liquid head (13m) | +1.8 |
| Vacuum | +1.0 / 0. |
| Vacuum vessel ($\Delta p_V$) | -1.0[(a)] / +0.85[(c)] kg/cm$^2$ |
| Weight (Pb converter @~8$\lambda$) : | |
| Barrel | 3500 tons |
| Endcap | 1000 tons each |
| Material | Aluminum alloy A5083-O |

(a) normal operation, (b) evacuation, (c) liquid argon spill-out

*Cryostat structure*: We show the cross-sectional view of the calorimeter in Fig.1. The characteristics of the Barrel design are; dished heads, two inner cylinders in the LAr vessel, radial-stay plates connecting the two inner cylinders to the outer-most cylinder of the LAr vessel, and washers penetrating the hadronic (HAD) and the electromagnetic (EM) modules. The Endcaps also have dished heads, inner cylinders (we are discussing to have one or two) and washers. Dished heads are effective to distribute the stress and to make the wall thickness thinner. The two inner module-support cylinders also support the LAr heads, further making the head wall-thickness thinner by reducing the effective vertical span of the wall. The radial-stay plates provides longitudinal strength and assist the inner cylinders in supporting module gravity loads. The washers contribute to

both vessel and module support, and help to maintain the whole calorimeter round. The radial-stay plates add dead area in the azimuthal angle ($\phi$) obviously, no such plates are used in the EM section. If the plates in the HAD1 section cause serious trouble, we will investigate an alternative plan to remove all the plates in the HAD1 section while the plates in the HAD2 section are kept. We put the thin washer in the EM section to make the inner-most Barrel LAr cylinder thin and yet to be strong against bucking. In this design, the EM and the HAD modules will not contribute to the vessel's structural strength.

This SDC Calorimeter design provides relatively thin vessel walls, convenient module installation and support, and allows dis-assembly access to the modules for maintenance, if necessary. The wall thicknesses we have at present are shown in Fig.2. The most up-to-date radial dimension of the Barrel is given in Fig.3, which are subject to change as SDC subsystem trade-off decisions are made.

*Support of the whole calorimeter*: A conceptual design for cold mass and vacuum shell supporting legs is given in Fig.4. The LAr vessels of the Barrel and the Endcap calorimeters are supported with the legs on the sides of the vessel cylinder. The calorimeter is placed on a rigid carrier and slides into final position. The carrier also will be an utility housing such as cryogenic valves, vacuum system, etc. The liquid argon calorimeter by itself will need no magnetic-flux return-yoke close to the calorimeter.

*Assembly and close-out*: A close-out scheme is presented in Fig.5. When modules are being assembled into the LAr vessel, the vessel is reinforced with the steel "girder rings" placed around the outermost LAr cylinder (Fig.5(a)) and the whole vessel will be rotated on the roller-supporter. After the module assembly, the LAr heads will be attached and the weight is transferred from the "girder" to the cold mass support (Fig.5(b)). The LAr vessel, then, slides into the outer Vacuum vessel which is on the rigid carrier (Fig.5(c)). The heads of the Vacuum vessel will then be attached and the close-out is finished.

## *3. Design of the modules*

In this section, we present segmentation of the EM and HAD modules in the longitudinal and transverse directions, number of readout channels and the channel capacitances. We discuss the basics of the speed of response and derive requirement for the cable length, etc. We also discuss the basics of the equivalent noise charge and derive level of the thermal noise. Finally, we present electrical readout scheme, cable connections, and location of preamps.

### *3.1 Segmentation*

*Segmentation*: We show the lateral segmentation of the modules in Fig.6. We employ the basic tower segmentation of $\Delta\eta=\Delta\phi=0.05$ in $\eta$ and $\phi$ directions. Within a tower, a longitudinal section of the EM module is further subdivided into $\Delta\eta=\Delta\phi=0.025$. The finer segmentation is to have a position resolution of less than 5mm for the electromagnetic showers. The segmentation maintains $\Delta\eta=\Delta\phi=0.05$ until the physical tower width becomes a value approximately equal to the FWHM EM shower width at shower maximum (about 100mm), after which the tower width remains constant. The $\phi$ division is set to 128 in $2\pi$ in the Barrel. In the Endcap, $2\pi$ in $\phi$ is divided into 1/16 symmetric sectors and segmented into towers in a sector as shown in the fig.6. In the Endcap, 2 meter is the radius for the physical size of a tower be 100mm in $\phi$. Over the 2m radius the sector is divided into 8, and inside the 2m radius the sector is divided so that the tower width remains constant (about 100mm) in $\eta$ and $\phi$.

The longitudinal segmentation is shown in Fig.7. A tower is modularized into 3 blocks, EM, HAD1 and HAD2. The EM module is further divided into one "massless" and two EM calorimeter sections. The "massless" gap is made of G10 pc boards only. One EM calorimeter section is subdivided into 4 to have $\Delta\eta=\Delta\phi=0.025$ segmentation. HAD1 and HAD2 are not divided further in the sense of readout. They are, however, "interleaved" into several preamps so that failure in a preamp will not kill the whole HAD1 or HAD2 section. The interleaving is also required to have an acceptable capacitance for one preamp. The interleaved outputs are extracted out of the cryostat and ganged into one readout channel.

*Number of readout channels*: The number of readout channels are counted and summarized in Table 2. When an EM or HAD module of a tower is divided by the washers, we count the channel separately for each modules. We have about 70k EM and 28k HAD, 98k in total, readout channels. These are "Data Acquisition" number of channels. When number of cables from the cryostat are in question, number of "interleaving" should be counted for the HAD sections.

To trigger the calorimeter, we propose an idea of the following trigger tower formation. Since 128 is the number (in $\phi$) and 8 is a divisor, we take a sum of 8x8 ($\Delta\eta x\Delta\phi$=0.4x0.4) towers as a trigger tower. In $\eta$ there are 98 towers, including the Endcap, and we form 12 trigger towers. In $\phi$ we form 16 trigger towers (there is a detail in the Endcap but let's ignore here). We also have triggers for the EM and HAD separately. The number of basic trigger towers is 384. To cover the boundaries between the trigger towers, we further form another 3 layers of the trigger towers, which are half-overlapped. As a result, we will have 1536 trigger channels.

Table 2. Number of readout channels

| Cal. | EM modules | HAD modules |
|---|---|---|
| Barrel | 45568 | 13312 |
| Endcap | 12432x2=24864 | 7184x2=14368 |
| Total | 70432 | 27680 |
| Grand total | 98112 | |

*Detector Capacitances*: We have calculated the detector capacitance according to the above segmentation and plotted the values in Fig.8. The inner radius of the EM module was 2.15m for the calculation and is slightly smaller than the proposed 2.25+$\alpha$(walls, vacuum, clearance...) in the EOI. Typical capacitances of the longitudinal segments are summarized in Table 3.

Table 3. Detector capacitances (nF)

| $\eta$ | "massless" | EM1 | EM2 | HAD1 | HAD2 |
|---|---|---|---|---|---|
| | | Barrel | | | |
| 0.0 | 0.30 | 0.44 | 4.1 | 12.0 | 21.2 |
| 0.5 | 0.35 | 0.50 | 4.6 | 13.7 | 24.1 |
| 0.9 | 0.44 | 0.65 | 5.9 | 17.5 | 30.9 |
| | | Endcap | | | |
| 1.5 | 0.43 | 0.61 | 5.2 | 11.9 | 16.2 |
| 2.0 | 0.27 | 0.38 | 3.2 | 7.3 | 9.9 |
| 2.5 | 0.22 | 0.30 | 2.6 | 5.9 | 8.0 |

*3.2 Speed of response*[4]

*Basics*: A schematic for the response at various stages is shown in Fig.9. Before the charge-amp the vertical axis is the current, and after the amp the voltage. At the detector capacitance the current in time is a triangle with a width of drift time, $t_d$. It is the best to integrate over the whole drift time, however, it is not necessary to do so because the peak current is at the beginning and effect of cutting the tail enters slowly.

In a real situation, a large electrode capacitance is connected to a preamplifier with a cable or a transmission line. Its effect is to slow down the transfer of the charge from the detector capacitance into the preamplifier due to the inductance of the connection. The peak of the current is now at $t_r$, named as the charge transfer time. To have a stable integrated charge, it is desirable to have the charge transfer time well less than the peaking time of the impulse response of the shaping, $t_p$. The requirement for the fast speed is the requirement for the short peaking time, and, then, the requirement for the fast charge transfer time.

Cables have inductance and capacitance. The inductance contributes to the charge transfer time while the cable capacitance contributes to the equivalent noise charge (ENC) due to the thermal noise of the preamplifier. Two choices are possible. One is to require the cable capacitance to be much smaller than the detector capacitance so as ENC to be the smallest,

effectively only due to the detector capacitance. The other is to allow a large cable capacitance determined by other requirement such as the required cable length and not to care about its contribution to ENC. The latter is possible if the sum of the detector and the cable capacitance is smaller than the capacitance allowed from the total ENC requirement.

In the following we think of the magnetic transformer coupling (MT) and the electrostatic transformer coupling (EST). The EST coupling is a new idea, in which the detector cells are connected in *series* compared to the conventional parallel ganging. The effect is the reduction of the detector capacitance by $1/n^2$ of parallel ganging when $n$ cells are connected in series. Since detector capacitance is reduced, the requirement for the cable inductance will be relieved and also ENC will be reduced. This is a good news. The bad news is non-linear response in the $n$ cells and large cross-talk to the adjacent towers. In the conventional ganging, the cross-talk is the ratio of the cross-talk capacitance to the high voltage blocking capacitance. The cross-talk capacitance is usually less than 10% of the detector capacitance and the blocking capacitance is more than 10 times larger than the detector capacitance. Thus the cross-talk is usually less than 1%. On the other hand, in the EST, the blocking capacitance is a detector cell seen from the cell in the $n$ cells and the cross talk is about 10%. In reality, the capacitance network of the EST coupling is not as simple as the conventional coupling and requires simulation to have a realistic response[5].

In the MT coupling, the ferrite-core transformer will be placed in front of the preamps. The effect of the MT is not for speeding up the response but for reducing ENC by reducing the total capacitance of detector and cable. We seek the smallest ENC in the MT coupling while in the EST we seek a long cable length, so long we can put the preamps out of the cryostat.

*The MT coupling*: If the charge transfer time is longer than the propagation time through the line ($t_r > t_{pd}$), the inductance of the line dominates the transmission line effects. The charge transfer time is approximately given as

$$t_r = 3.5\sqrt{LC_D}$$

where $C_D$ is the detector capacitance and $L$ is the sum of inductance in the connection. $L$ is consisting of the inductances between the electrode to the transmission line ($L_{DC}$), of the transmission line ($L_C$), and the stray inductance ($L_S$) as shown in the equivalent circuit. We require;

$$t_r \le t_p/f_r \text{ and } C_c \le C_D/f_c$$

where $C_C$ is the capacitance of the transmission line. The factors $f_r$ and $f_C$ express the requirements for the fast response and for the small contribution of cable capacitance to ENC. We take $f_r$=2 and $f_C$=3 for the numerical calculations. The derived characteristics of the transmission line are tabulated in Table 4.

The propagation time through the line, $t_{pd}$, is given as

$$t_{pd} = \sqrt{L_c(C_c + C_D)} = \frac{t_r}{3.5}\sqrt{1 + \frac{1}{f_c}}\ .$$

As stated, $t_{pd}<t_r$ , and the tabulated relations should be valid for $f_C \ge 0.1$. Since we can not make an infinitely wide transmission line, there is a practical minimum cable inductance (let it be $L_O$) and we have a limit on the maximum detector capacitance to be connected as;

$$C_D \le \frac{1}{L_{DC} + L_o + L_s}\left(\frac{t_p}{3.5 f_r}\right)^2 .$$

*The EST coupling*: We dismiss the $f_C$ relation and, instead, take the cable length $l_C$ as a parameter. The derived characteristics of the transmission line are listed in Table 5. In the expressions the detector capacitance $C_D$ is the capacitance of the parallel ganging and $n$ is the transformer ratio ( $n$ cells in series). When $C_D$ becomes small, $L_C$ becomes large and $C_C$ small. Practically, this trends are cut at a limit of a twisted pair cable, e.g. $Z_O$=110Ω which has a 0.95μH/m unit inductance and a 80pF/m unit capacitance, as an example. Then the propagation time through the line is;

$$t_{pd} = \sqrt{L_c C_c} = 8.7(ns/m)l_c$$

The range $t_r < t_{pd}$ should be valid for $l_c \leq 5.7$m (@$t_p$=100ns). For the cable length more than this we require simulations for the response and relations.

Table 4. Derived cable characteristics for the MT coupling

| | |
|---|---|
| Requirements: $t_r \leq \frac{t_p}{f_r}$ , $C_c \leq \frac{C_D}{f_c}$ | |
| then, $t_r = 3.5\sqrt{LC_D}$ ; $L = L_{DC} + L_c + L_s$ | |
| $L_c = \frac{1}{C_D}\left(\frac{t_p}{3.5 f_r}\right)^2 - L_{DC} - L_s$ , $\left(L_c > L_o \Rightarrow C_D < \frac{1}{L_o + L_{DC} + L_s}\left(\frac{t_p}{3.5 f_f}\right)^2\right)$ | |
| $Z_0 = \sqrt{\frac{L_c}{C_c}} \cong \frac{\sqrt{f_c}}{C_D}\left(\frac{t_p}{3.5 f_r}\right)$ | |
| $l_c = 3 \times 10^8 \sqrt{\frac{L_c C_c}{\varepsilon_r}}$ | |
| $t_{pd} = \sqrt{L_c(C_c + C_D)} = \sqrt{L_c C_c}\sqrt{1 + \frac{C_D}{C_c}} \cong \frac{t_r}{3.5}\sqrt{1 + \frac{1}{f_c}}$ | |
| where | |
| $t_r$: charge transfer time | $t_p$: peaking time |
| $L_{DC}$: detector-cable inductance | $L_c$: cable inductance |
| $L_S$: stray inductance | $Z_O$: characteristic impedance |
| $l_c$: cable length | $t_{pd}$: propagation delay |
| $\varepsilon_r$: relative dielectric constant | $L_O$: minimum cable inductance |

Table 5. Derived cable characteristics for the EST coupling

Requirements:

$t_r \le \frac{t_p}{f_r}$ , $l_c$ *fixed*

then

$$L = L_{DC} + L_c + L_s \equiv L_c$$

$$L_c = \frac{n^2}{C_D}\left(\frac{t_p}{3.5 f_r}\right)^2 \le 3.8\,\mu H^{(*)}$$

$$C_c = \left(\frac{l_c}{3 \times 10^8}\right)^2 \frac{\varepsilon_r}{L_c} \ge 320 pF^{(*)}$$

$$Z_o = \sqrt{\frac{L_c}{C_c}}$$

$$t_{pd} = \sqrt{L_c C_c} = \frac{\sqrt{\varepsilon_r}\, l_c}{3 \times 10^8}$$

where (*) assumes $Z_O$=110Ω twist-pair cables ($dL/dl$=0.95μH/m, $dC/dl$=80pF/m) and the cable length 4m.

Numerical values of the cable characteristics are summarized in Table 6 for the detector capacitance at $C_D$=5nF. The numbers are listed for two shaper impulse-response peaking times of 100ns and 50ns. The limitations on the cable length and the detector capacitance are $l_c \le 1.2$m and $C_D \le 12$nF for $t_p$=100ns, and $l_c \le 0.5$m and $C_D \le 5$nF for $t_p$=50ns. Although the required speed should be determined from the physics point of view, we take 100ns as the design criteria for the moment.

Table 6. Cable characteristics at $C_D$=5nF for $t_p$=100ns and 50ns

| | $t_p$=100ns | | $t_p$=50ns | |
|---|---|---|---|---|
| | MT | EST[a] | MT | EST[a] |
| $L_c$[b] | 37nH | 1020nH | 6nH | 255nH |
| $C_c$ | 1.7nF | 0.7nF | 1.7nF | 2.8nF |
| $Z_o$ | 4.7Ω | 38Ω | 1.9Ω | 9.5Ω |
| $t_{pd}$ | 15.9ns | 30.3ns | 6.4ns | 27.6ns |
| $l_c$ | 1.2m | 4.0m | 0.5m | 4.0m |
| max.$C_D$ | 12nF[c] | | 5nF[d] | |

(a) $n$=5 and $l_c$=4m are fixed

(b) $L=L_{DC}+L_c+L_s$ where $L_{DC}$=2nH and $L_s$=2nH are assumed

(c) $L_o$=12.6nH (symmetric ground: $w/h$=10mm/0.2mm and $l$=1m)

(d) $L_o$=6.3nH (symmetric ground: $w/h$=10mm/0.2mm and $l$=0.5m)

*3.3 Thermal noise*

*Equivalent Noise Charge (ENC)*: We assume a conventional JFET input charge preamplifier. An equivalent circuit is given in Fig.10. The capacitance $C_O$ is the sum of all the capacitances in front of the preamps, such as detector, cross-talk, and cable. The capacitance $C_{GS}$ is the capacitance of the control electrode of the transistor. We can express the equivalent noise charge due to the intrinsic series noise of the amplifying device as follows. If a charge $q_S$ is induced on the capacitance $C_O$, then the charge on the control electrode $C_{GS}$ will be $q_S C_{GS}/(C_O+C_{GS})$. Then, the equivalent noise charge induced on the capacitance $C_O$ by the noise charge due to the series noise voltage $\langle v_G^2\rangle=4kTR_S$ on the capacitance $C_{GS}$ is;

$$\langle q_{sn}^2\rangle=\left(\frac{C_o+C_{GS}}{C_{GS}}\right)^2\cdot C_{GS}^2\,4kTR_s=4kTR_s(C_o+C_{GS})^2=4kT\frac{a_n}{g_m}(C_o+C_{GS})^2$$

$$=4kTa_n\frac{t_{el}}{C_{GS}}(C_o+C_{GS})^2=4kTa_nt_{el}C_o\left(\sqrt{\frac{C_o}{C_{GS}}}+\sqrt{\frac{C_{GS}}{C_o}}\right)^2$$

where we have used the relations $R_s=a_n/g_m$ ($a_n$=2/3 for JFET) and $g_m=C_{GS}/t_{el}$. $g_m$ is the transconductance and $t_{el}$ is the electron channel transit time ($t_{el}$=0.5ns is being taken).

The factor

$$f=\left(\sqrt{\frac{C_o}{C_{GS}}}+\sqrt{\frac{C_{GS}}{C_o}}\right)$$

is called the capacitance mismatch factor, and the minimum is 2 if matched ($C_O=C_{GS}$). The matching condition can be achieved with the magnetic transformer or with the eletrostatic transformer by transforming the capacitance $C_O$ into $C_O/n2$ where $n$ is the transformer ratio. The matching ratio is given by $n=\sqrt{C_O/C_{GS}}$.

The optimum noise is the noise passed through the CUSP or approximately the triangular shaping, and $ENC_{opt}^2=\langle q_{sn}^2\rangle/t_p$ where $t_p$ is the zero-to-peak time (impulse response peaking time). When the bipolar shaping of $m$ integrations is used, $ENC$ is about 1.4 times larger than $ENC_{opt}$ ($m$=1~4).

The net result is

$$ENC=1.4\sqrt{4kTa_n}\sqrt{\frac{t_{el}}{t_p}}\sqrt{C_o}\cdot\frac{f}{n}=0.658\left(\frac{f}{2}\right)\sqrt{\frac{T(K)}{300}}\frac{1}{n}\sqrt{C_o(nF)}\ fC$$

for $t_p$=100ns at the input of charge preamp. When matched, the transformer ratio is $n$=32 at $C_o$=10nF and $C_{GS}$=10pF.

In the above argument, the feedback capacitance $C_f$ does not play any role. The equivalent circuit for the charge amplifier can be written as shown in Fig.10. The charge is transferred into the capacitance $C_{GS}$ first, and then it is transferred on to the feedback capacitance $C_f$ within the amplifier response time $R_{in}(C_{GS}+C_O)$.

We have neglected the parallel noises, such as the shot noise, 1/f noise, dielectric noises. Among the available devices, JFET has the best over-all characteristics in the shot and 1/f noises which can be neglected. Bipolar transistors has larger shot noise due to the larger base current. MOSFET

or Gallium-arsenide FET (MESFET) or modulation doped FET (MODFET) have larger 1/f noise.

*Energy scale*: To convert the equivalent noise charge into the equivalent noise energy ("thermal noise in energy unit"), we require the energy scale stating how much of charge is seen at the input of charge preamp by unit incident energy. The general formula is

$$\frac{dQ_o}{dE} = s \cdot \left(\frac{p}{\mu}\right) \cdot \frac{1}{W_i} \cdot \frac{1}{2} \cdot \left(\frac{Q}{Q_o}\right) \cdot \left(\frac{C_B}{C_D + C_b}\right) \cdot \frac{1}{n}$$

where $s$ is the energy-loss sampling fraction in the liquid argon for the minimum ionizing particle, which is specific for the sampling cell structure, $(p/\mu)$ is the so-called $(e/\mu)$-ratio for electrons and $(h/\mu)$-ratio for hadrons (e.g. pions), $Wi$ is the energy required to ionize the Ar atoms ( the ionization potential), the factor 1/2 is for observing only electrons of the ion-electron pairs, $Q/Q_O$ is the charge collection ratio, $C_B/(C_B+C_D)$ is the charge sharing ratio between the detector and the high voltage blocking capacitances and $n$ is the transformer ratio. The $(p/\mu)$-ratio is also specific for the cell structure but the dependence is small and we assume here $(e/\mu)$=0.6 and $(h/\mu)$=0.4. These are a conservative choice to see less charges. $W_i$ is 25eV. $Q/Q_O$ is $0.9t_p/t_d(2\text{-}t_p/t_d)$ where the factor 0.9 is due to recombination and the latter factor is due to the charge integration up to the peaking time $t_p$ (for $t_p<t_d$). $C_B/(C_B+C_D)$ is 0.9 for $C_B$ being 10 times $C_D$.

Taking the sampling cell structure as shown in Fig.3, we have the sampling fraction $s$=0.13 for the EM section and $s$=0.044 for the HAD section. The resulting energy scales are

$$\frac{dQ_o}{dE} = 202\frac{t_p}{t_d}\left(2 - \frac{t_p}{t_d}\right)\frac{1}{n}\ fC/GeV = \frac{88.4}{n} fC/GeV \quad (EM)$$

and

$$\frac{dQ_o}{dE} = 49\frac{t_p}{t_d}\left(2 - \frac{t_p}{t_d}\right)\frac{1}{n}\ fC/GeV = \frac{21.4}{n} fC/GeV \quad (HAD)$$

for $t_p$=100ns and $t_d$=400ns.

*Thermal noise in energy unit*: Combining the equivalent noise charge and the energy scale, we have the thermal noise in energy unit as

$$\sigma_E = 0.00744\left(\frac{f}{2}\right)\sqrt{\frac{T(K)}{300}}\sqrt{C_o(nF)}\ GeV \quad (EM)$$

and

$$\sigma_E = 0.0308\left(\frac{f}{2}\right)\sqrt{\frac{T(K)}{300}}\sqrt{C_o(nF)}\ GeV \quad (HAD)$$

for $t_{el}$=0.5ns (JFET of $g_m$=20mS and $C_{GS}$=10pF) and $t_p$=100ns. We show the noises for the unmatched and matched cases with magnetic transformer (MT) coupling in Fig.11. We take the temperature $T$=100K assuming the preamps are in the liquid argon, and the capacitance $C_O$ to be the sum of the detector capacitance $C_D$, the cross-talk capacitance $0.1C_D$, the cable capacitance $C_C$=$C_D$/3 and the detector-to-cable capacitance $C_{DC}$=0.2nF. We also show the noises for the EST coupling in Fig.12. In the small detector capacitance region, the noise is dominated by the cable capacitance and is flattened. Further studies are planned to simulate the electric responses and the noises to be more realistic.

*3.4 Basic design of the modules*

*Interleaving:* Since a HAD section has a too-large capacitance for the fast response and single preamp for a HAD section has danger to lose the section in case of preamp death, we divide a section into several elements. By alternatively connecting the electrodes to the separate preamps ("interleaving"), the danger of losing a whole HAD section is spread thin. The interleaving is better than dividing the section into longitudinal segments as far as the dividing number is small since in the HAD section the electromagnetic component of the hadronic shower deposits energy in a limited longitudinal depth.

The capacitance of 12nF is the maximum for $t_p$=100ns. The HAD1 section will be interleaved into 2 and the HAD2 section into 3 in the Barrel (similar in the Endcaps). The signal cables from each preamps are extracted out of the cryostat and the number of cables required are about 2.5 times the number of HAD readout channels.

*Connection and location of preamps*: In the MT coupling, the maximum cable length is to be less than 1.2m from the electrodes to the preamps. Since the height of the HAD1 and HAD2 modules is about 0.9m, ganging cable will be placed on the both sides of the wedge-shaped modules (a module is made of two towers), and preamps will be placed in the back of the modules in the Barrel calorimeter.

While the modules in the Barrel are tilted 3 degrees to avoid the gap between the modules to be a crack, in the Endcap region the polar angle $\theta$ is so small that the tilting will not help. A plan is to have a fan-shaped modules with a height of the fan to be about 1meter. Each readout board of the cell has transmission line to the outer peripheral and ganged at the peripheral where preamps will be located. The transmission lines in cells are ganged in parallel, requirement for the cable inductance can be multiplied by the number of cells. From the point of view of radiation damage, the fan-shaped and peripheral location of preamps is desirable since the radiation decreases rapidly as the angle is going away from the beam axis. Schematics for the Barrel and the Endcap module are shown in Fig.13.

## *4. Summary*

The liquid argon calorimeter has good characteristics such as radiation resistance, ease of calibration, long-term stability, etc. to be a candidate calorimeter in the SSC environment. Recognizing that the engineering issues are critical, we have been working on and have proposed a specific design of the liquid argon calorimeter.

FEM analysis is proceeding for the structure and wall thickness. Support scheme of the whole calorimeter has been emerging, together with the assembly and close-out schemes.

Lateral and longitudinal segmentations are defined and the number of readout channels and capacitances are deduced. The number of readout channels is about 98k.

The slow drift velocity is the fundamental but the critical limiting factor for the fast response is the charge transfer time, $t_r$, from the detector to the preamps together with the intrinsic thermal noise. Requiring $t_r<t_p/2$

where $t_p$ is the peaking time of the impulse response of the shaper, cable length are required to be less than 1.2m and the maximum detector capacitance to be less than 12nF for the practically smallest thermal noise at $t_p$=100ns in the magnetic transformer (MT) coupling.

With the matched magnetic transformer coupling and a bipolar shaping, the thermal noises are <4MeV in the "massless" gap, <4MeV in EM1, <15MeV in EM2, <100MeV in HAD1 and <130MeV in HAD2, resulting in the total noise of <165MeV per tower, and <130MeV per 8x8 EM and <1.3GeV per 8x8 HAD trigger tower. The electrostatic transformer coupling (EST) with the transformer ratio of 5 and the cable length of 4m gives twice or more thermal noise, which is dominated by the cable capacitance in the small detector capacitance region ($C_D$<5nF).

A scheme for a module shape, number of interleaving, connections between detector elements and preamps, and preamp locations are being developed.

---

[1]F.Abe, K.Amako, S.Inaba, H.Ikeda, M.Ikeda, H.Iwasaki, N.Ujiie, Y.Unno(contact person), K.Ogawa, N.Kanematsu, A.Kusumegi, T.Kondo, Y.Sakai, Y.Takaiwa, T.Haruyama, H.Hirayama, A.Maki, K.Tsukada/KEK, Y.Watanabe, T.Tanimori/Tokyo Inst. Tech., K.Nishikawa/INS,Tokyo Univ., K.Kuboyama et al./Kawasaki Heavy Ind.
[2]Summary report on an engineering design study of a hermetic liquid argon calorimeter for the SSC, T.Adams et al, Martin Marietta, Jan.(1990)
[3]An Air-Core Solenoid detector, presented by T.Kondo, KEK-Preprint 89-191
[4]V.Radeka, Ann. Rev. Nucl. Part. Sci. 38(1988)217
[5]M.Levi, LBL memorandum

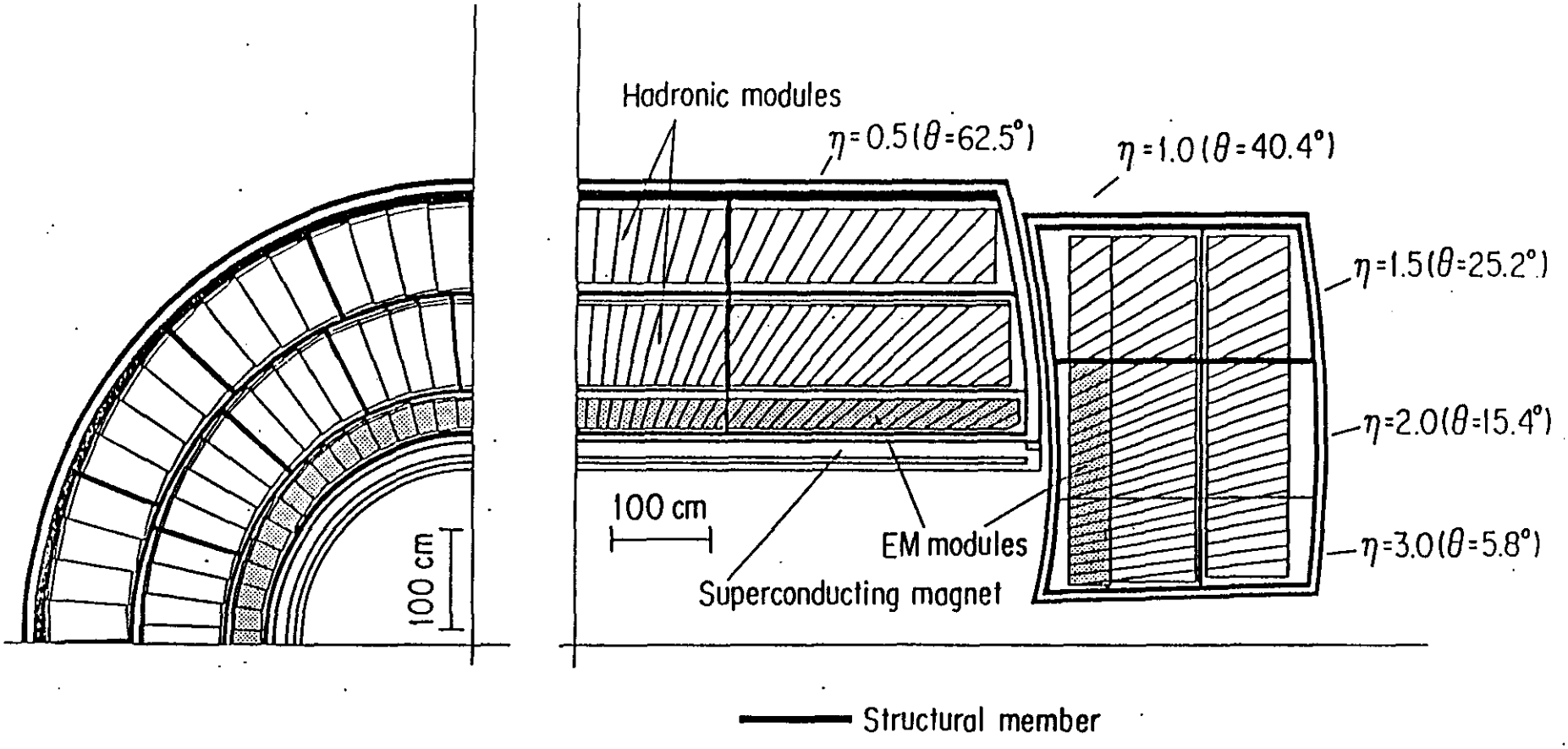


Liquid Argon Calorimeter for SSC

Fig. 1 Cross-sectional view of the LAr Calorimeter

1990. 6. 20

# Cryostat Wall thickness

- Washer / Stays are added
- Positive pressure in the vacuum layer included

... and still in progress

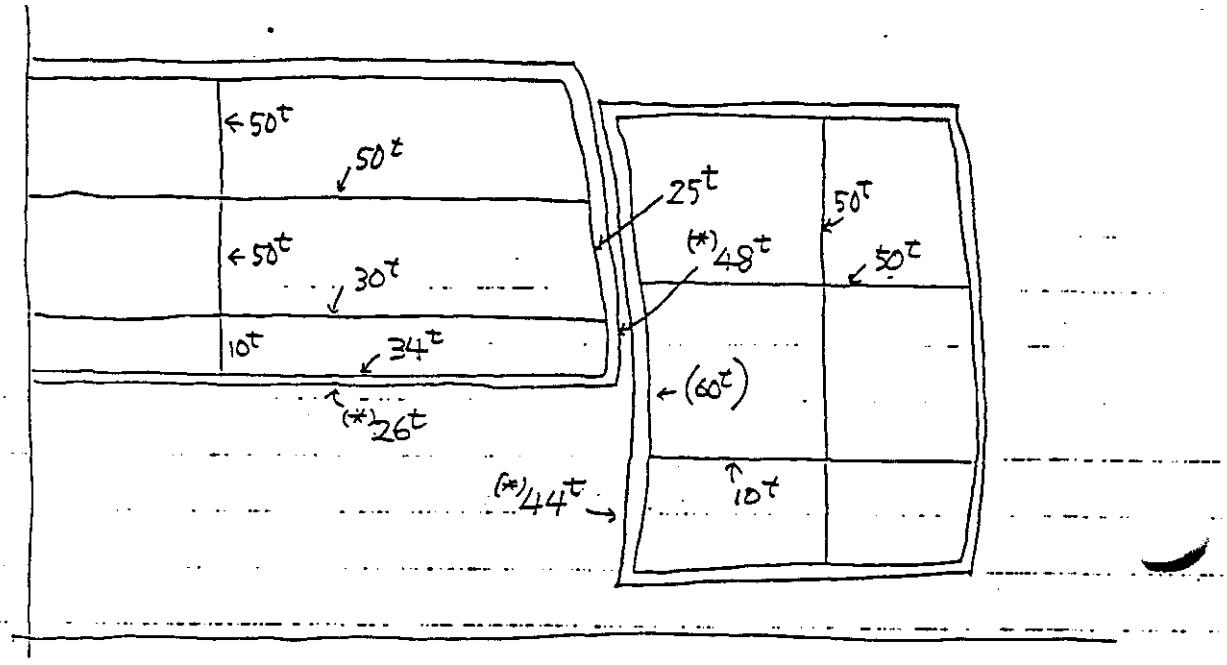


(*) Vacuum layer ±0.85 kg/cm² (12 psi) by LAr spill
Instability calculated !

Fig. 2 Cryostat wall thickness (at present)

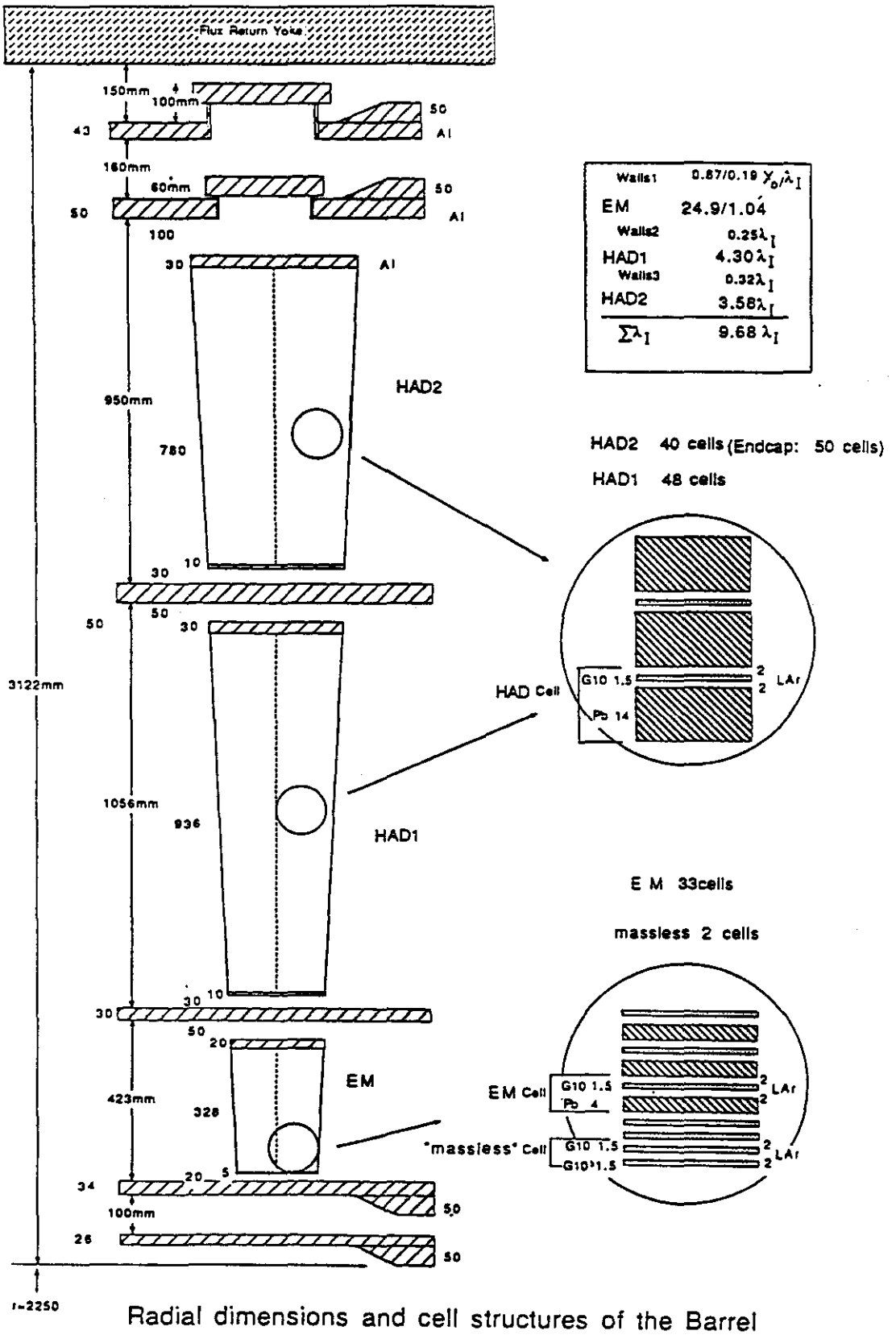


Radial dimensions and cell structures of the Barrel

Fig. 3 Radial dimension of the Barrel

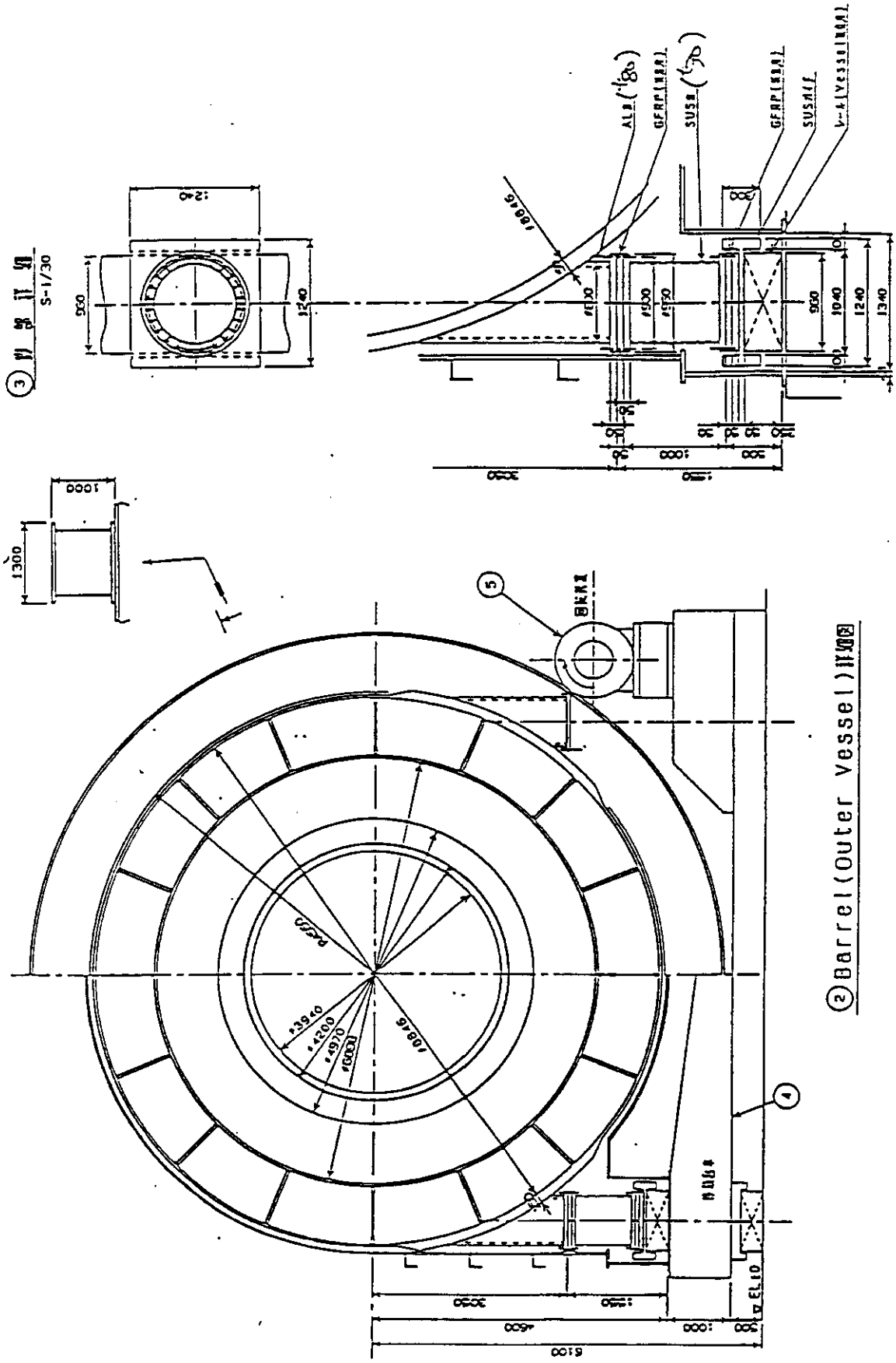


Fig. 4 A conceptual design for cold mass and vacuum shell supporting

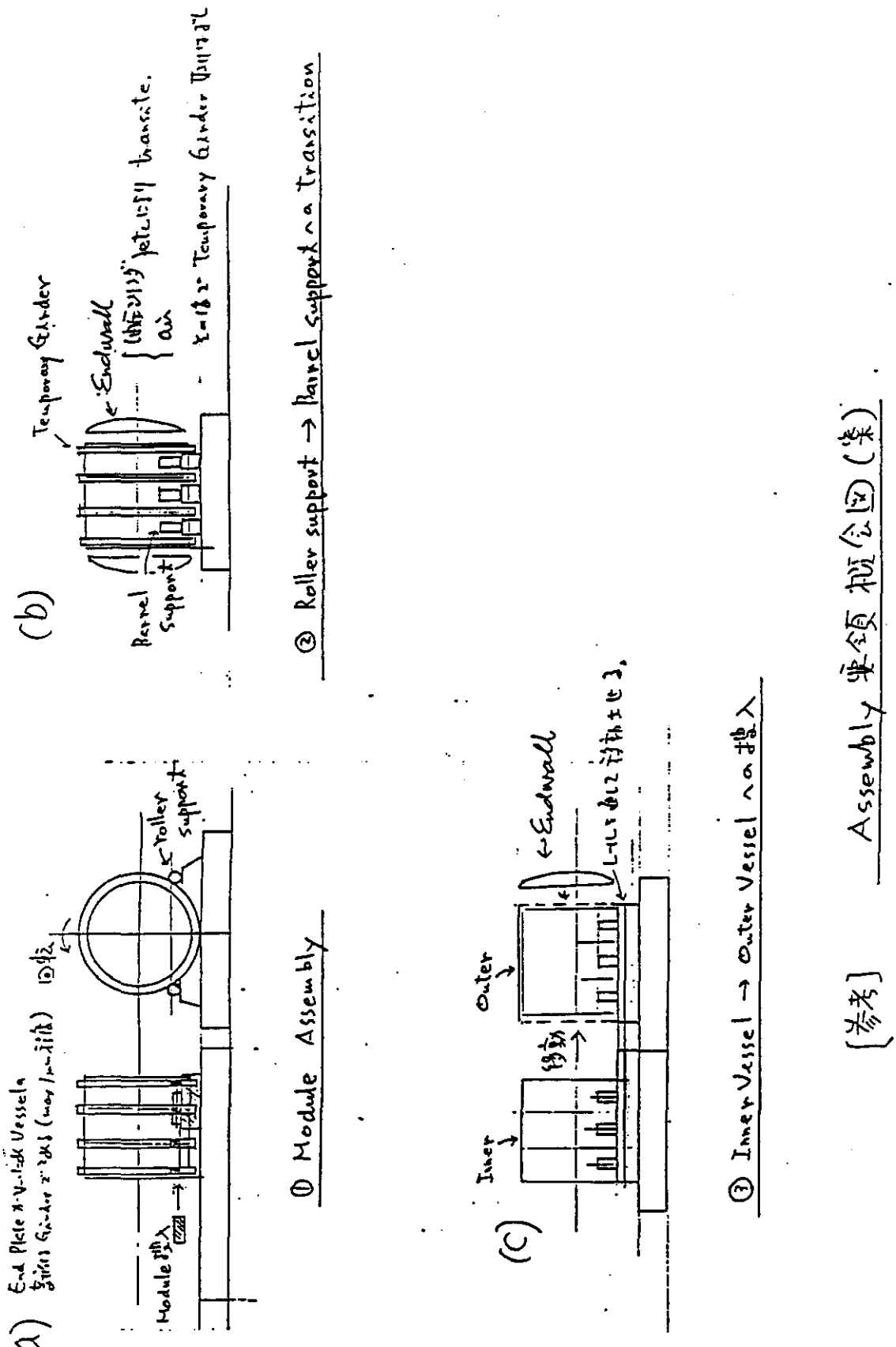


Fig. 5 Concepts for assembly and close-out; (a) module insertion, (b) head assembly and weight transfer from "girder rings" to the cold mass support, and (c) slide-in into the vacuum vessel and attaching heads.

A07006-(1) A4 ±45

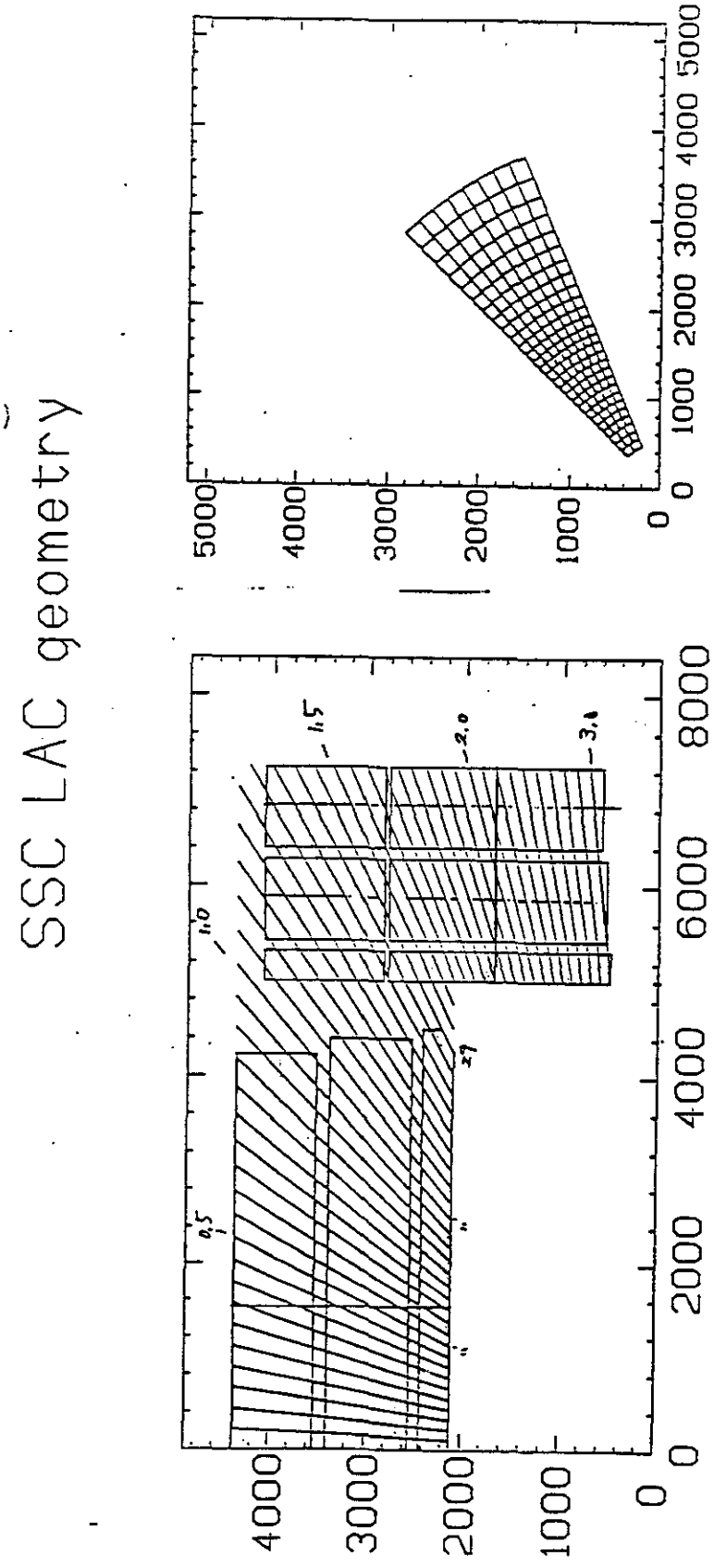


Fig. 6 Lateral segmentation of the modules of the Barrel and the Endcap

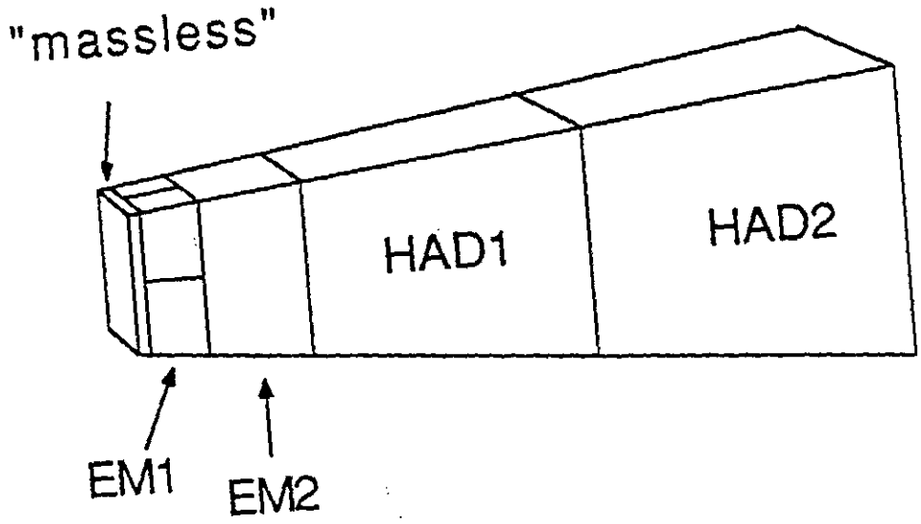


Basic longitudinal segmentation of a tower

Fig. 7 Basic longitudinal segmentation of a tower

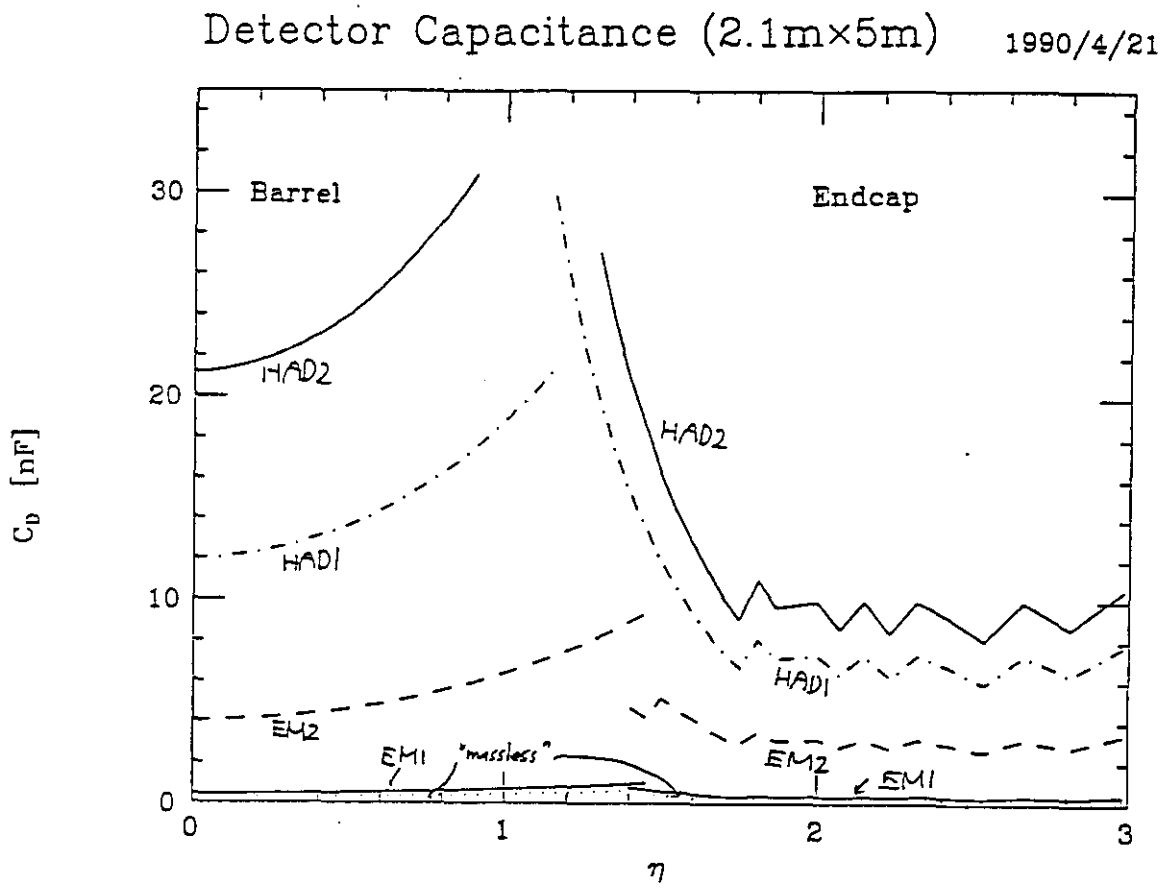


Fig. 8 Detector capacitances as a function of pseudorapidity, $\eta$

1990, 4, 22

Relations between the cable characteristics and the detector capacitance

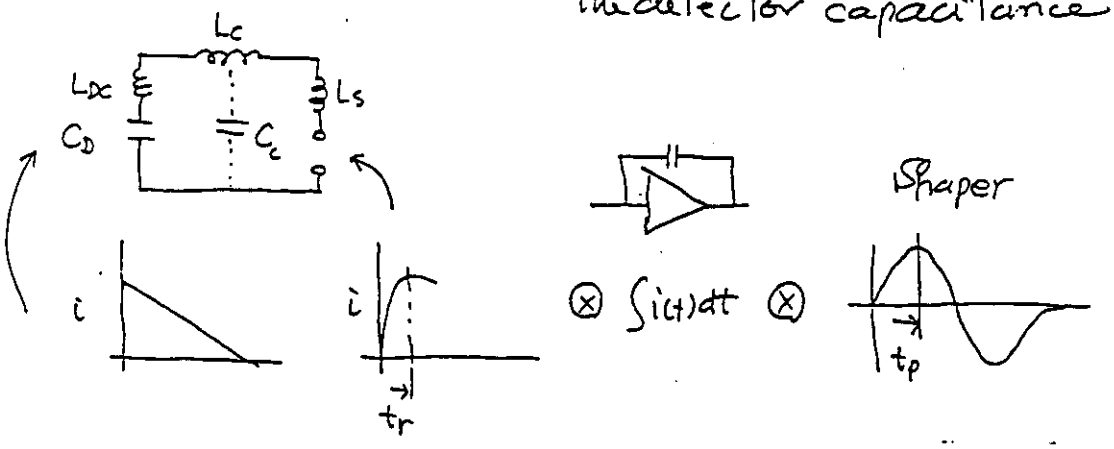


Fig. 9 Speed of response: schematics at various stages

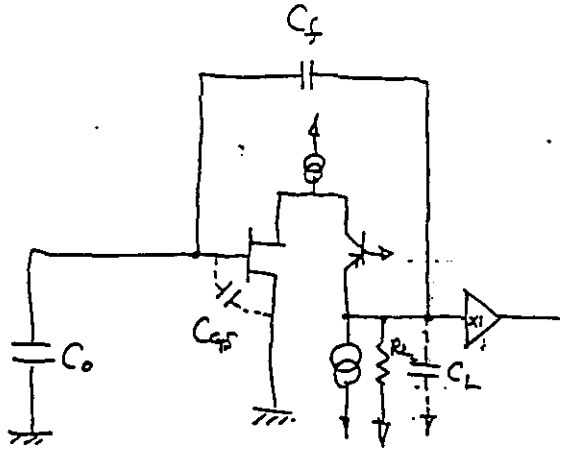


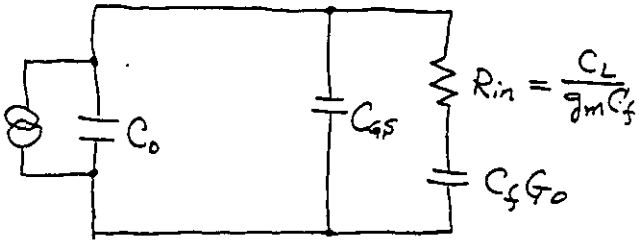


$G_0 = g_m R_L$ : open-loop gain

Fig. 10 A schematic of a detector and a charge preamplifier and an equivalent circuit diagram

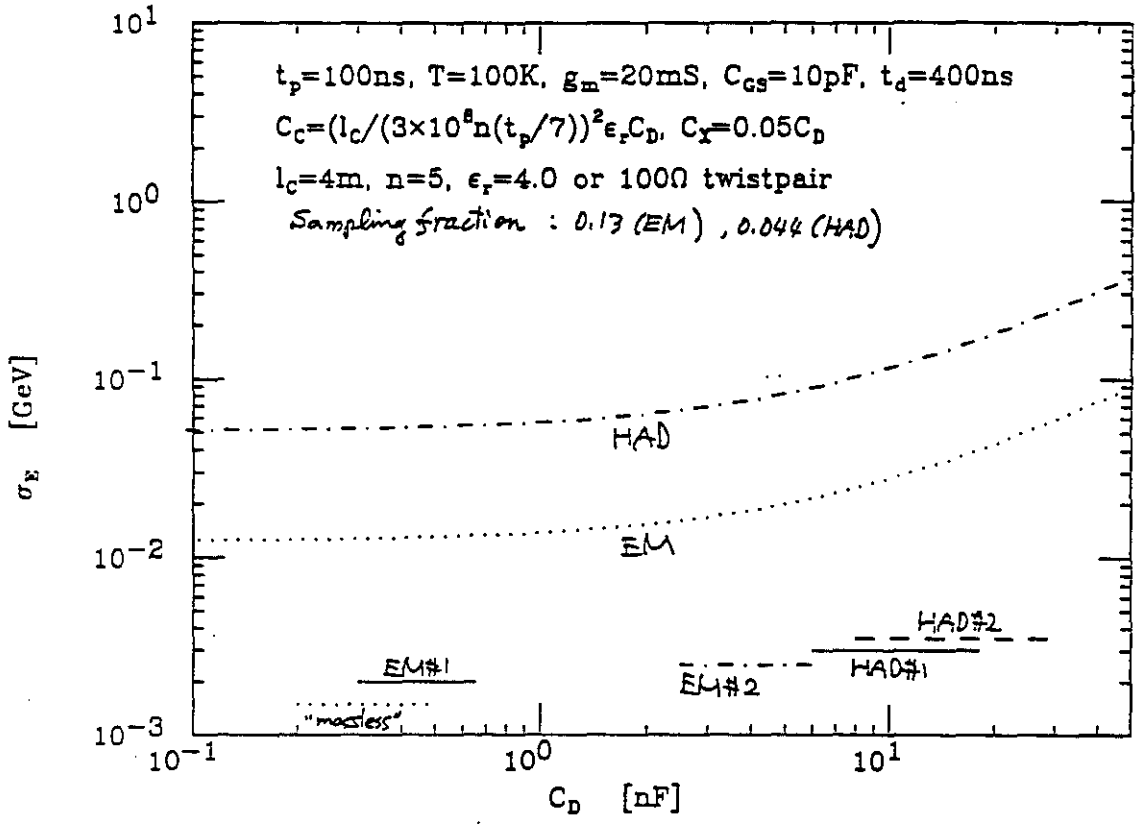


Fig. 12 Thermal noise with electrostatic transformer; dots/EM and dotdash/HAD.

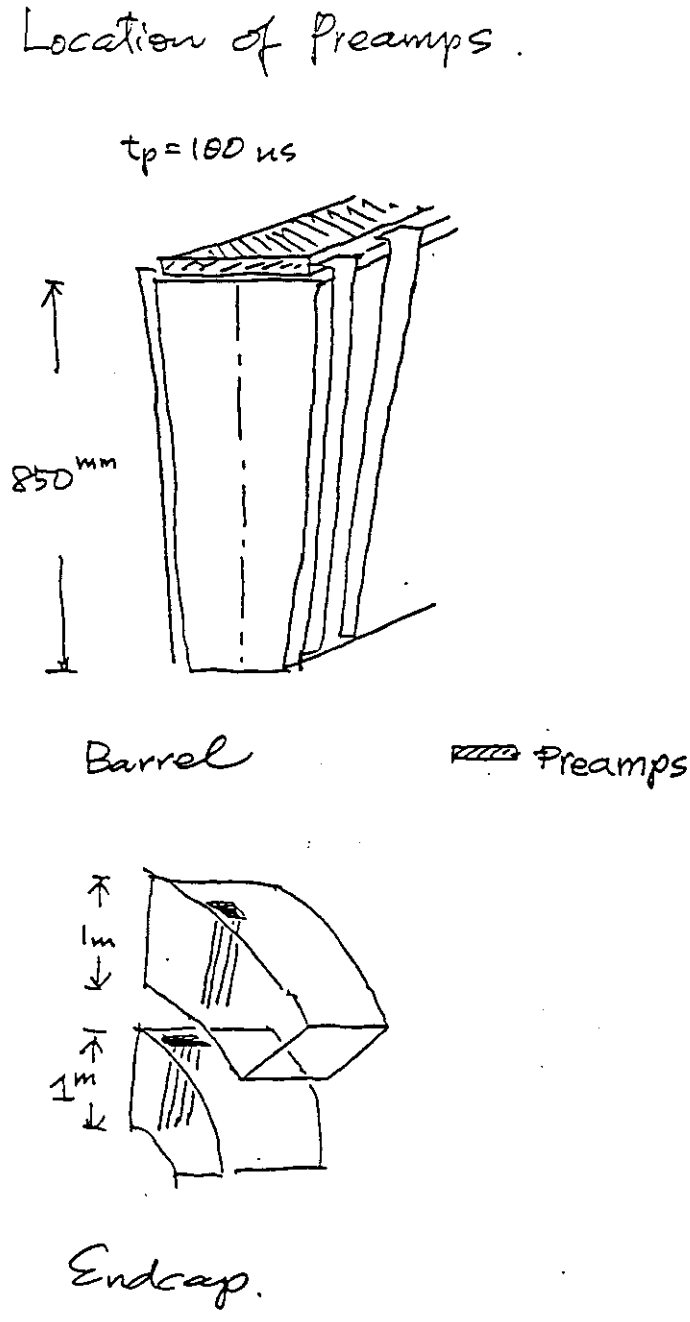


Fig. 13 Concept for the location of preamps and cables from detector elements to preamps